Radiation Effects in Single-Walled Carbon Nanotube Thin-Film-Transistors

Cory D. Cress, *Member, IEEE*, Julian J. McMorrow, *Student Member, IEEE*, Jeremy T. Robinson, Adam L. Friedman, and Brian J. Landi

***Abstract*—The fabrication, characterization, and radiation response of single-walled carbon nanotube (SWCNT) thin-film field effect transistors (SWCNT-TFTs) has been performed. SWCNT-TFTs were fabricated on SiO_2-Si substrates from 98% pure semiconducting SWCNTs separated by density gradient ultracentrifugation. Optical and Raman characterization, in concert with measured drain current I_{on}/I_{off} ratios, up to 10^4, confirmed the high enrichment of semiconducting-SWCNTs. Total ionizing dose (TID) effects, up to 10 MRads, were measured *in situ* for a SWCNT-TFT under static vacuum. The results revealed a lateral translation of the SWCNT-TFT transfer characteristics to negative gate bias resulting from hole trapping within the SiO_2 and SiO_2-SWCNT interface. Additional TID exposure conducted in air on the same device had the opposite effect, shifting the transfer characteristics to higher gate voltage, and increasing the channel conductance. No significant change was observed in the device mobility or the SWCNT Raman spectra following a TID exposure of 10 Mrad(Si), indicating extrinsic factors dominate the transfer characteristics in the SWCNT-TFT devices during irradiation. The extrinsic effects of charge trapping and the role that gas adsorption plays in the radiation response are discussed.**

***Index Terms*—Carbon electronics, carbon nanotube field effect transistor, radiation effects, SWCNT-TFT, total ionizing dose (TID).**

I. Introduction

THE past decade has witnessed tremendous advances in carbon-based nanoelectronics, most notably in regards to single-walled carbon nanotube (SWCNT) and graphene-based field effect transistors (FETs) [1]–[5]. The promise of SWCNTs for future high-performance electronics and for use in radiation environments stems from the material's unique structural and electronic properties. SWCNTs are single-atom-thick tubular structures consisting of sp^2 hybridized carbon. The delocalized π electrons in the sp^2 bonds lead to extremely high mobilities along the axial direction [6], thereby enabling high-frequency operation [1]. Though challenges still exist for carbon-based nanoelectronics, the extraordinary electronic properties and the promise of enhanced-radiation tolerance, make SWCNT-based devices one of the front-runners for "beyond silicon" technologies.

Structurally, SWCNTs are an open honeycomb lattice with low density, low atomic number, and small cross section, which make SWCNT-based devices attractive for use in radiation environments. The small cross section results in a lower probability of incident particle strikes, and in the case of a particle incidence, the short path length (i.e., the diameter of the SWCNT) and low-density lead to a minimal amount of ionizing energy transfer. For instance, time-dependent density functional theory-based simulation results indicate that the maximum electronic energy transfer (ionizing energy loss) to a SWCNT by an incident proton is less than 100 eV [7]. This translates into a maximum charge generation of about 10 aC for a SWCNT with a 0.75 eV bandgap if half of the energy is converted into carriers in the first excited state. This upper limit charge is similar to that which would be stored on the most aggressively scaled SWCNT devices (having a diameter of 1 nm, gate oxide thickness of 5 nm, and channel length of 10 nm) under a 1 V gate bias. Thus, charge transient propagation to subsequent devices and the observation of single event upsets will likely remain inconsequential until the extremely aggressive scaling regime is reached.

Recent reports indicate that cumulative radiation exposure effects, including those related to ionizing energy absorption [known as total ionizing dose (TID)] and crystalline damage [known as displacement damage dose (DDD)] play a role in the observed radiation response of SWCNTs, either by directly damaging the SWCNTs (DDD) [8]–[11] or by affecting the properties of the surrounding materials which lead to changes in the overall device behavior (TID) [12]. Typically, the onset of damage is not observed until very high DDD (e.g., 10^{13} MeV/g) is imparted to the material [13]. For DDDs that are comparable to aerospace environments, SWCNT thin-film-transistors (SWCNT-TFTs) have demonstrated high radiation tolerance [14]. Likewise, high tolerance to TID exposure (6 Mrad Co-60 irradiation) has recently been reported for SWCNTs-TFTs [15]. However, very high 1.3-MeV gamma-particle doses (in excess of 16 Mrad) have led to changes in the reported SWCNT structural properties, probed via Raman spectroscopy [16]. Until additional research is conducted, TID effects will continue to be a concern for SWCNT-based devices due to radiation induced changes in the surround materials of the device, resulting from trapped charges or Schottky barrier

Manuscript received July 17, 2010; revised August 27, 2010; accepted August 27, 2010. Date of current version December 15, 2010. This work was supported in part by the Defense Threat Reduction Agency MIPR #10-2197M. The work of C. D. Cress was supported by the NRL Karles Distinguished Scholar Fellowship program. The work of A. L. Friedman was supported by the National Research Council.

C. D. Cress, J. T. Robinson, and A. L. Friedman are with the Electronics Science and Technology Division, U.S. Naval Research Laboratory, Washington, DC 20375 USA (e-mail: carbon.electronics@nrl.navy.mil).

J. J. McMorrow is with Global Strategies Group (North America) Inc., Crofton, MD 21114 USA.

B. J. Landi is with the Chemical and Biomedical Engineering Department, Rochester Institute of Technology, Rochester, NY 14623 USA.

Color versions of one or more of the figures in this paper are available online at http://ieeexplore.ieee.org.

Digital Object Identifier 10.1109/TNS.2010.2078515

height modification at the source and drain contacts [12]. This extrinsically induced radiation response can be convoluted with environmental factors [17], [18] making it challenging to elucidate the radiation-induced effects. In particular, SWCNT-based devices can be highly sensitive to molecular adsorbates (e.g., O_2 or H_2O) leading to large gate hysteresis, loss of electron transport, and threshold voltage shifts [19], [20], which can mask radiation-induced changes if not properly controlled. Therefore, paramount to the identification of the basic radiation-response mechanisms of SWCNT-based devices is the deconvolution of the device response manifested from intrinsic and extrinsic material and device properties [13].

An ideal platform for assessing the radiation response of SWCNT-based devices is a structure in which large quantities of test samples are readily produced, all with consistent performance. This would allow rapid characterization of devices exposed to different conditions without concern for sample-specific results. Such studies are required to identify the root cause of specific radiation-induced performance degradation. Most notably, the development of a scalable SWCNT-device fabrication process for achieving high-density *alignment* of SWCNTs with *uniform electronic properties* has not been forthcoming due to the large distribution of SWCNT diameters, chiralities, and concomitant electronic properties that are obtained during synthesis. However, continual research in these areas has established two encouraging advances that significantly address these engineering issues. Chemical vapor deposition (CVD) growth of perfectly aligned SWCNTs has led to SWCNT-TFT devices fabricated from such ensembles which show high mobilities (up to 850 cm^2/Vs) and good high-frequency performance [4], [21], [22] However, these devices suffer from poor I_{on}/I_{off} ratios due to a significant metallic SWCNT fraction. Therefore, it is critical that the SWCNT-sample inhomogeneity be addressed to produce "electronically" pure SWCNTs. To date, the most promising approach for enriching the electronic types from as-synthesized materials is through the use of density gradient ultracentrifugation (DGU) [23]. This process yields highly purified semiconducting SWCNTs by a subtractive procedure and has proven useful for creating SWCNT-TFTs with some of the best DC [24] and microwave characteristics [25] reported to date.

Though engineering challenges exist for the widespread commercialization of these carbon-based nanoelectronics, there is still much to be ascertained about their fundamental radiation response. With this objective, the radiation response of benchmark SWCNT-based nanoelectronic devices was investigated. SWCNT-TFTs were fabricated using 98% pure semiconducting SWCNT samples prepared by the DGU method. The electrical performance of the devices is consistent with recently reported SWCNT-TFT devices. Furthermore, an *in situ* analysis of the radiation response of the device following incremental Co-60 gamma-ray TID exposures, both under vacuum and in air, was employed to assist in deconvoluting intrinsic and extrinsic radiation response mechanisms. The results ascertained from this work represent the first step towards understanding the complex radiation response mechanisms of SWCNT-TFTs.

II. Experimental

A. SWCNT-TFT Device Fabrication

SWCNT-TFTs were fabricated from 98% IsoNanotube-S semiconducting SWCNTs purchased in powder form from NanoIntegris, Inc. A 0.01 mg/mL suspension of SWCNTs in a 1% (w/v) sodium dodecyl sulfate aqueous solution was prepared by horn sonication (10 W) for 20 min. Using the filter-transfer method developed by Rinzler's group [26], a thin-film of the SWCNTs was formed on a p-type (1–10 ohm cm) Si wafer with a 1000 Å thermal oxide. Following photolithographic patterning (Shipley S1811) the SWCNT-network channel regions were isolated using a 10 s O_2 plasma etch, followed by stripping the photoresist with acetone, and a "thermal cleaning" step (2 hr heat treatment at 300°C in air). Source-drain lithographic patterning and metallization (20 Å Ti/380 Å Au) via electron-beam evaporation then followed. Hundreds of devices were formed with channel length and width varying from 2 to 64 μm and 4 to 128 μm in steps of powers of two, respectively, resulting in 36 unique device dimensions.

Fabricated chips were mounted into 16-pin ceramic packages with Ag paint to enable *in situ* testing. Source/drain contacts were wire bonded with the substrate serving as a global back gate.

B. Characterization and Irradiation Conditions

Electrical characteristics of the CNT-TFTs were measured using a Keithley 4200-SCS semiconductor parametric analyzer, while Raman spectra were obtained using an Acton double monochromator and Si CCD detector with 532 nm diode laser excitation. The radiation studies were performed at the NRL Co-60 irradiation facility comprised of a 25 000 Ci Co-60 source housed at the bottom of a 10 ft pool. For doses up to 2000 krad(Si) a dose rate of 0.240 krad(Si) was used, which was increased to 1.2 krad/s for the 5000 and 10 000 TID irradiations. Devices were mounted within the test chamber and electrically connected to the parametric analyzer via coaxial cables housed within a plastic snorkel leading to the surface.

Multiple *in situ* measurements were performed on the same SWCNT-FET with a device channel length and width of 32 μm. Following connection in the test chamber, the dc device characteristics were monitored over time while the chamber was evacuated to a base pressure of 8×10^{-7} Torr for 16 h (as measured within the diffusion pumping system, actual sample chamber pressure was slightly higher) by which time reproducible transfer characteristics were obtained. The device characteristics remained unchanged following a 10 min period of static vacuum, during which the sample chamber was isolated from the pumping system.

During irradiation, the following dose/measurement procedure was iterated:

1) Apply gate bias of 2 V; drain current monitored $V_{ds} = 0.1$ V;
2) Insert sample chamber into calibrated dosing source position;
3) Expose device for desired dosing step time;

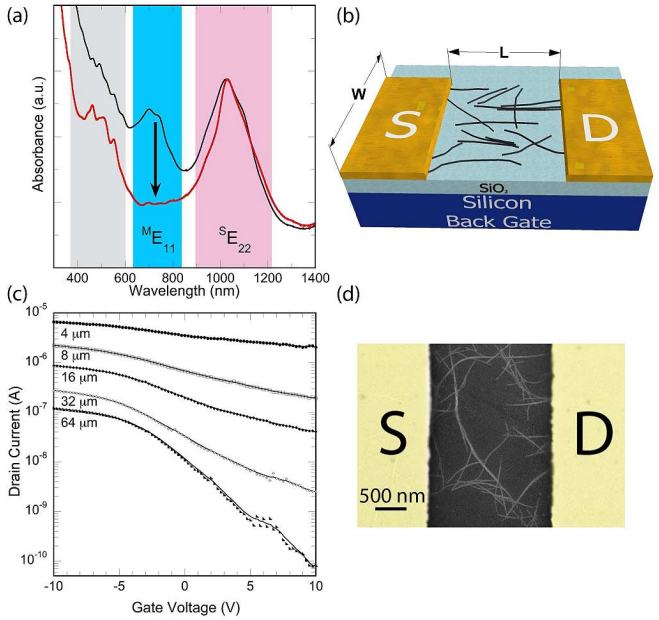

Fig. 1. (a) Optical absorbance spectrum of semiconducting enriched SWCNT suspended in a 1% (w/v) sodium dodecyl sulfate aqueous solution (red, bottom curve) overlaid with the SWCNT absorbance spectrum of the pure material prior to separation by electronic type via DGU (black, top curve). (b) Schematic illustrating the SWCNT-TFT back gated device structure. (c) SWCNT-TFT transfer characteristics for channel lengths of 4, 8, 16, 32, and 64 μm. (d) Representative SEM image of the SWCNT connected network bridging the source and drain contacts, which were emphasized with gold false coloring.

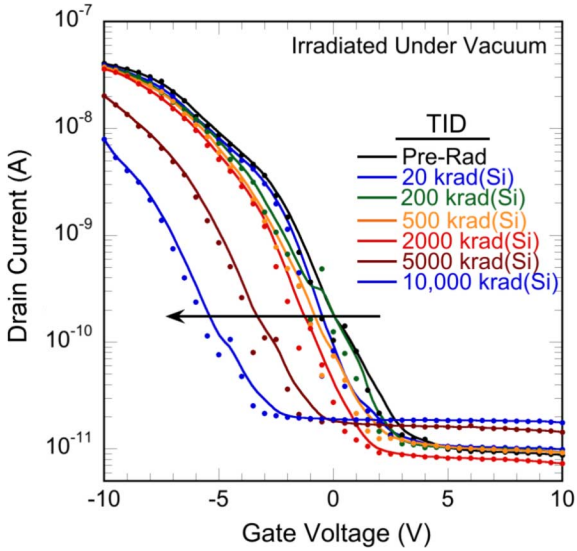

Fig. 2. CNT-TFT transfer characteristics as a function of total ionizing dose irradiated in vacuum. The dose rate was 240 rad(Si)/s except for the last two measurements, which were 1.2 krad(Si)/s.

4) Remove from source (4 ft), and allow device to equilibrate for 100 s;
5) Turn off gate bias and immediately conduct gate sweep;
6) Repeat until completed.

Following a TID of 10 000 krad(Si) the sample chamber was removed from the Co-60 pool and allowed to equilibrate following exposure to air. After equilibration (about 10 min) the above procedure was repeated while the same device was irradiated with an *additional* 500 krad(Si) TID, within a static-air environment.

III. Results and Discussion

A. SWCNT-TFT Device Performance

Fig. 1(a) shows a representative optical absorption spectrum for a solution of 98% semiconducting enriched SWCNTs suspended in a 1% (w/v) sodium dodecyl sulfate aqueous solution. The red (lower) trace is from the enriched material while the black (upper) trace is from the starting SWCNT material prior to separation by electronic type via DGU. The reduction of the absorption feature (blue middle region) shows clear evidence for the enrichment of semiconducting SWCNTs over that of the starting material. Fig. 1(b) provides a schematic representation of the device structure, while Fig. 1(d) contains a representative scanning electron micrograph depicting the SWCNT network bridging two Au (false colored) source/drain contact pads.

Fig. 1(c) depicts the transfer characteristics for five CNT-FETs with constant channel width (128 μm) and channel length increasing from 4 μm to 64 μm. The $I_{\rm on}/I_{\rm off}$ ratio (for $V_{g,\rm off} = +10$ V and $V_{g,\rm on} = -10$ V) steadily increases with channel length indicating an increased fraction of semiconductor SWCNT transport. For the shortest channel length a significant fraction of metallic conduction is present resulting in a device that cannot be gated into an off state when biased up to $V_g = 10$ V. With a $V_g = -10$ V applied, the back gate is able to lower the Fermi level of the semiconducting-SWCNTs to allow for hole-injection through the Schottky barrier formed at the semiconducting SWCNTs-Ti-Au metal contact and into the SWCNT channel. As a result, a superposition of the two conduction modes is observable. The on-state semiconducting conductivity and metallic conductivity contributions have a power law dependence on the device channel length (4 to 64 μm) with exponents of -1.34 and -3.54, respectively. Only for the longest channel length does the device become fully semiconductor like, ultimately reaching an $I_{\rm on}/I_{\rm off}$ of over 10^4. Of the $\sim$50 devices tested, the mobility ranged from 1.2 to 4.5 cm^2/Vs. This is consistent with recent results on SWCNT-TFTs comprised of SWCNT networks: 1–5 cm^2/Vs [27], 8 cm^2/Vs [28], and 5–20 cm^2/Vs [25]. The latter is most notable because they were comprised of densely aligned 99% semiconductor-enriched SWCNT (separated by the DGU method). The lower mobility for SWCNT-TFT devices, in comparison with individual SWCNT-FETs, has been attributed to both nanotube-nanotube coupling resistance and nanotube-nanotube electrostatic screening [25]. Debundling the SWCNTs may be key to mitigating both effects, since mobilities as high as 850 cm^2/Vs have been reported for CNT-TFTs comprised of densely aligned (7 tubes/μm) *and* nonbundled SWCNTs [4]. In general, the fabricated devices have successfully achieved the primary objective of a standard test platform for which radiation studies can be conducted.

B. SWCNT-TFT Radiation Response

Fig. 2 depicts the transfer characteristics of the wire-bonded SWCNT-TFT (32L/32W) measured *in situ* after incremental Co-60 gamma ray TID exposure. Prior to irradiation (black

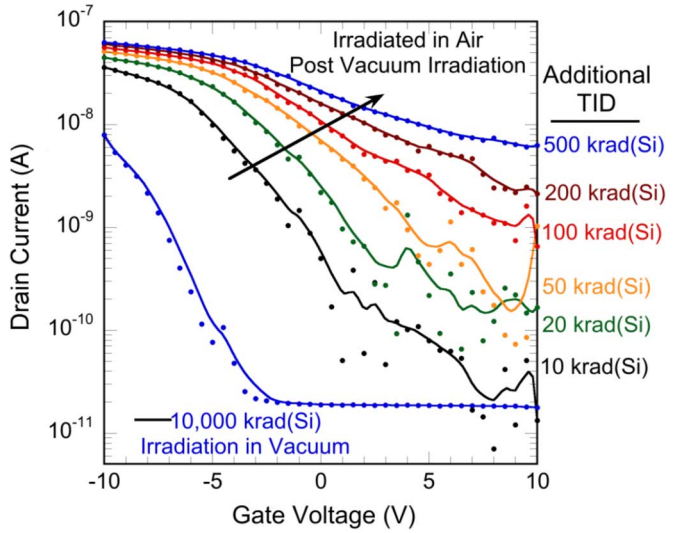

Fig. 3. CNT-TFT transfer characteristics as a function of *additional* total ionizing dose irradiated in air following the vacuum irradiation after drain current equilibration.

line/circles) the device shows good characteristics with an $I_{\rm on}/I_{\rm off}$ of 7000 and a mobility of 2.7 cm^2/Vs. There is a noise-free off region from $V_g = 4$–10 V which is only observed in these CNT-TFTs when under vacuum and less affected by gas molecules interacting with the surface. A gradual shift to negative gate bias is observed in the device characteristics with incremental TID. For the irradiating conditions employed ($V_g = 2$ V; $V_{\rm sd} = 0.1$ V) electrons generated within the SiO_2 are drawn towards the SiO_2-Si interface, while holes are driven to the SiO_2-SWCNT interface. Therefore, the observed shift is indicative of trapped holes in the SiO_2 near the SWCNT interface reducing the Fermi energy in the SWCNTs causing a bending (valance band shifts downwards) obstructing hole injection. For the final two TIDs [5000 krad(Si) and 10 000 krad(Si)] the dose rate was increased to 1.2 krad(Si)/s $(\sim 5 \times \text{greater})$ to minimize the dosing time since the device was under static vacuum.

Additional dosing of this same device in ambient air was performed to explore the role that gas molecules play on the observed radiation response. Fig. 3 depicts the final 10 000 krad(Si) transfer characteristics measured **in vacuum** along with those measured following the *additional* TID **in air** (labeled on the figure). After an additional 10 krad(Si), the effects of the ambient air are immediately apparent. Foremost, a shift of over 10 V is observed for the device to reach the full off condition, and the channel conductance increases by $50\times$. With additional TID up to 500 krad(Si), the trend continues with increased channel conductance and reducing $I_{\rm on}/I_{\rm off}$, and is consistent with recent *ex situ* experimental results on SWCNT-TFTs irradiated with Co-60 in air [15]. These trends, in addition to the increased noise observed in the subthreshold characteristics, are the result of SWCNT background doping and dynamic interactions between SWCNTs/SiO_2 with molecules in the air. As aforementioned, all atoms in the SWCNTs are surface atoms and are highly sensitive to adsorbed gas molecules. The SWCNT/gas interactions are discussed in more detail later.

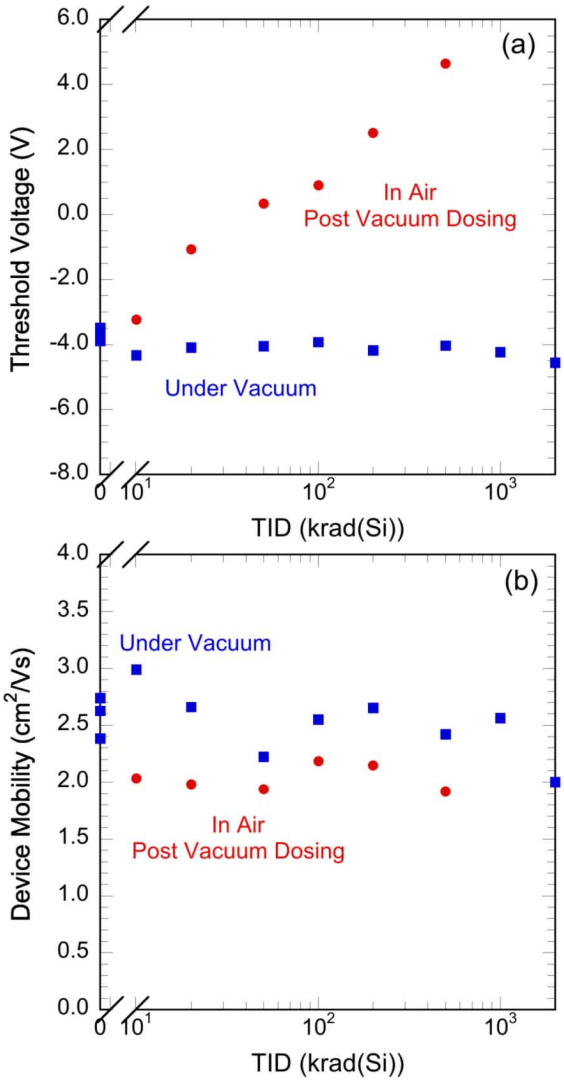

Fig. 4. (a) Threshold voltage. (b) Device mobility as a function of total ionizing dose irradiated in vacuum (blue squares) or *additional* total ionizing dose irradiated in air (red circles).

Comparisons between the threshold voltage V_T and mobility with TID exposure in vacuum (blue squares) and additional TID exposure in air (blue circles) are depicted in Fig. 4. The V_T is the V_g-axis intercept for a straight-line tangent to the measured transfer characteristics at maximum slope. Under vacuum, the V_T dips after the first dose recovers slightly, then again reduces slightly over the TID range, resulting in a total ΔV_T of -0.8 V after 2 Mrad(Si). The trend towards lower V_g is consistent with the subthreshold characteristics and reinforces the conclusion that trapped holes near the SiO_2-SWCNT interface are the dominant response mechanism. Based on historical Si-MOSFETs radiation response results, this effect can be ameliorated with the use of thinner gate oxides. In contrast, the V_T is logarithmically dependent on TID when irradiated in air, shifting to higher voltage with increasing TID. Therefore, a large V_g is needed to deplete/band bend the channel region to restrict hole concentration/transport. The total change in threshold voltage after an additional dose of 500 krad(Si) was $V_T = +7.9$ V and is over 37 times greater than the shift observed in air assuming the trend continues to 2 Mrad(Si).

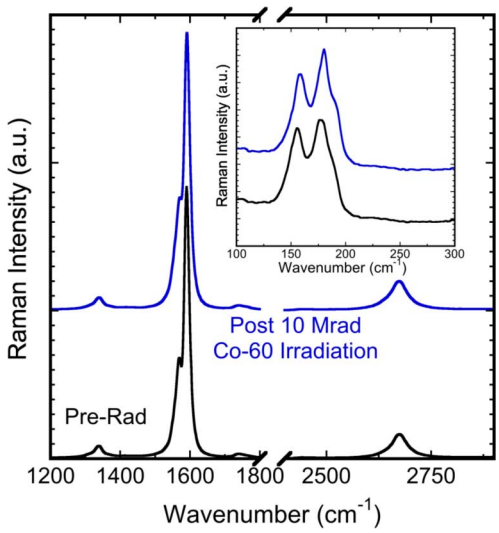

Fig. 5. Representative Raman spectra of a 98% semiconductor enriched SWCNT thin film pre- and post-irradiation in air up to 10 000 kRad. Inset: Radial breathing modes.

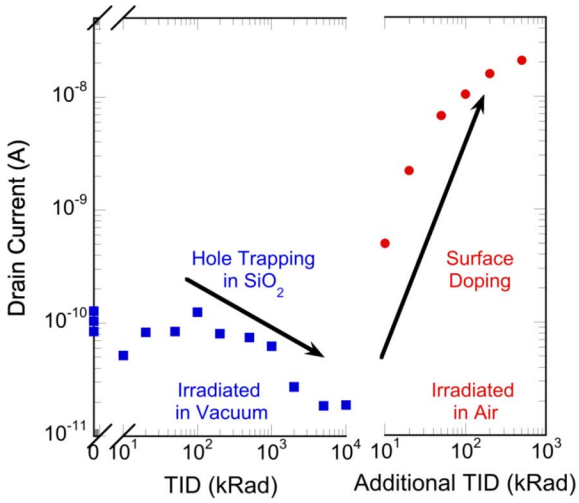

Fig. 6. Zero-bias drain current as a function of TID exposure in vacuum (blue squares) and as a function of *additional* TID exposure in air (red circles).

As illustrated in Fig. 4(b), irradiation of the CNT-TFT under vacuum and in air has little affect on the mobility of the device as both show a nearly constant trend up to a 500 krad(Si). This result indicates that irradiating the SWCNTs under these conditions does not create defects within the crystalline lattice of the material, but rather induces an extrinsic electric field that modifies the local potentials and carrier concentrations of the SWCNTs manifesting in the observed response.

This resilience of the SWCNTs during exposure in air is supported by Raman spectroscopy data conducted on test samples before and after exposure to a TID of 10 000 krad(Si) in air (unbiased), as shown in Fig. 5. The small peak at 1340 cm^{-1} (D-band) is related to defects, while the G-band peak at 1591 cm^{-1} is characteristic of sp^2-bonded carbons (i.e., graphite). The multi-Lorentzian lineshape for the G-band resonance from 1550–1620 cm^{-1} confirms the high degree of semiconducting enrichment in this sample. The small D:G ratio also indicates a low-defect content in the SWCNTs. A recent study on SWCNT papers showed no destruction of the SWCNTs after a dose of 5 Mrad(Si), but a small increase in D-band and G-band peak intensities in reference to the D-band overtone (2674 cm^{-1}) was observed [16]. The small increase that was observed in the D-band peak intensity may have manifested from the larger SWCNT volume probed by the laser in the bulk SWCNT paper, but such spectral changes were not observed in the present radiation study.

The inset in Fig. 5 depicts the radial breathing modes of the SWCNTs, which correspond with the cooperative vibration of the carbon atoms normal to the SWCNT axis. The diameter of the SWCNTs are inversely proportional to the energy of these peaks resulting in a diameter distribution ranging from 1.3 to 1.6 nm [18]. The similarity in the spectra pre- and post-TID of 10 000 krad(Si) indicates that the changes observed in the electrical characteristics are not the result of radiation induced defects disrupting the crystalline nature of the SWCNTs.

The equilibrium carrier concentration of the SWCNTs is directly related to the zero-bias drain current (I_{D0}) and monitoring its fluctuations with TID can assist in understanding the radiation-induced changes observed in the device performance. Fig. 6 illustrates the evolution in I_{D0}, which shows a peaked response that "traces" the pre-radiation transfer curve as if it were simply shifted laterally toward negative gate bias (this small feature is present and laterally shifted in all $I_d - V_g$ measurements conducted under vacuum). This type of behavior results from trapped carriers within the SiO_2 that induce equal and opposite charges that are divided between the SWCNT and the Si back gate. Trapped charges near the SWCNT surface cause the greatest shift in Fermi level of the SWCNTs and corresponding gate bias needed for the gate to mirror all of the trapped charge allowing the Fermi level to return to the unperturbed level. Based on the magnitude of ΔV_T (-0.8 V), the SiO_2 trap surface density can be estimated (assuming they are predominately at the SiO_2 :SWCNT interface) to be $\sim 3.6 \times 10^{11}$ holes/cm^2.

In air, the opposite response is observed in which the zero-bias drain current rapidly increases with additional TID, finally reaching an I_{D0} that is 200× greater than the pre-irradiation value. Shifting the transfer characteristics to higher gate bias indicates localized *negative* trapped charges near the SWCNT surface perhaps through the presence of electron traps/hole donating gas molecules in the proximity of the SWCNTs or SiO_2 surface. Oxygen [29], water [19], and water/oxygen redox couples [20] have been identified as potential charge accepting species that may become weakly adsorbed on the surface of the SWCNTs resulting in p-type doping. Adsorption of these molecules during irradiation is likely one of the dominant mechanisms. In addition, silanol terminated SiO_2 is known to bind water on the surface through hydrogen bonding [19] and can result in multilayer water coatings. Therefore, the exposed SiO_2 surface in the SWCNT-TFTs may also contribute to the observed changes by adsorbing water and serving as electron traps or by stabilizing other electron trapping molecules (oxygen). Charges on the SiO_2, at greater distance, are less effective at modulating the SWCNT carrier density, but the large number that can be present may make it another important factor in the observed response. The aforementioned mechanisms can be present with or without TID exposure, and in fact, V_T shifts to higher gate bias are commonly observed in pristine device tested in air. However,

the magnitude of the shift is much less ($\Delta V_T < 1$ V) and occurs over a longer time scale (days). Therefore, it is possible that the radiation induced charge generation in the gate SiO_2, and subsequent transport to the surface by the *in situ* biasing conditions accelerate the surface doping processes.

IV. Conclusion

A systematic study has been undertaken towards deconvoluting the complex radiation response of SWCNT-based nanoelectronics. In the present paper, SWCNT-TFT comprised of 98% semiconductor-enriched SWCNTs with p-channel behavior were fabricated and shown to scale consistently with long-channel FETs. The $I_{\rm on}/I_{\rm off}$ ratios (approaching 10^4) and mobilities were shown to be comparable to typical SWCNT-TFT technologies. The use of *in situ* electrical characterization was a critical aspect of the work as it enabled the effects of TID imparted to the device in vacuum and in air to be assessed independently. In vacuum, the transfer characteristics shift by $\Delta V_T = -0.8$ V after a TID of 2000 krad(Si), while the mobility remains nearly constant within the uncertainty of the data. This effect is consistent with positive SiO_2 and interface trapped charge build-up. In contrast, additional TID exposure in air up to 500 krad(Si) on the same device resulted in a $\Delta V_T = +7.9$ V shift to higher gate bias. Hole doping by water and oxygen directly adsorbed on the surface of the SWCNTs or by electron traps bound to the surface by silanols are the dominant factors causing the dramatic changes observed in the device characteristics during TID exposure in air.

Acknowledgment

The authors would like to thank J. Mann for electrical fixturing/testing support, and H. Hughes, P. McMarr, S. Buchner, and D. McMorrow for helpful discussions of the manuscript. C. D. Cress also acknowledges M. Ganter for his SWCNT characterization efforts.

References

[1] L. Nougaret, H. Happy, G. Dambrine, V. Derycke, J.-P. Bourgoin, A. A. Green, and M. C. Hersam, "80 GHz field-effect transistors produced using high purity semiconducting single-walled carbon nanotubes," *Appl. Phys. Lett.*, vol. 94, no. 24, p. 243505, Jan. 1, 2009.

[2] X. Wang, X. Li, L. Zhang, Y. Yoon, P. K. Weber, H. Wang, J. Guo, and H. Dai, "N-doping of graphene through electrothermal reactions with ammonia," *Sci.*, vol. 324, no. 5928, pp. 768–771, May 8, 2009.

[3] A. N. Pal and A. Ghosh, "Ultralow noise field-effect transistor from multilayer graphene," *Appl. Phys. Lett.*, vol. 95, no. 8, p. 082105, Jan. 1, 2009.

[4] S. J. Kang, C. Kocabas, T. Ozel, M. Shim, N. Pimparkar, M. A. Alam, S. V. Rotkin, and J. A. Rogers, "High-performance electronics using dense, perfectly aligned arrays of single-walled carbon nanotubes," *Nature Nanotech.*, vol. 2, no. 4, pp. 230–236, Apr. 1, 2007.

[5] Q. Cao, H.-S. Kim, N. Pimparkar, J. P. Kulkarni, C. Wang, M. Shim, K. Roy, M. A. Alam, and J. A. Rogers, "Medium-scale carbon nanotube thin-film integrated circuits on flexible plastic substrates," *Nature*, vol. 454, no. 7203, pp. 495–500, Jan. 1, 2008.

[6] P. Avouris, Z. Chen, and V. Perebeinos, "Carbon-based electronics," *Nature Nanotech.*, vol. 2, no. 10, pp. 605–615, Oct. 1, 2007.

[7] A. V. Krasheninnikov, Y. Miyamoto, and D. Tomanek, "Role of electronic excitations in ion collisions with carbon nanostructures," *Phys. Rev. Lett.*, vol. 99, no. 1, p. 016104, Jan. 1, 2007.

[8] B. Smith and D. Luzzi, "Electron irradiation effects in single wall carbon nanotubes," *J. Appl. Phys.*, vol. 90, no. 7, pp. 3509–3515, Jan. 1, 2001.

[9] V. Skakalova, A. B. Kaiser, U. Dettlaff, K. Arstila, A. V. Krasheninnikov, J. Keinonen, and S. Roth, "Electrical properties of C4+ irradiated single-walled carbon nanotube paper," *Phys. Status Solidi B*, vol. 245, no. 10, pp. 2280–2283, Jan. 1, 2008.

[10] A. Tolvanen, G. Buchs, P. Ruffieux, P. Gröning, O. Gröning, and A. V. Krasheninnikov, "Modifying the electronic structure of semiconducting single-walled carbon nanotubes by Ar^+ ion irradiation," *Phys. Rev. B*, vol. 79, no. 12, pp. 1–13, Mar. 1, 2009.

[11] F. Banhart, J. X. Li, and A. V. Krasheninnikov, "Carbon nanotubes under electron irradiation: Stability of the tubes and their action as pipes for atom transport," *Phys. Rev. B*, vol. 71, no. 24, p. 4, Jun. 1, 2005.

[12] X. Tang, Y. Yang, W. Kim, Q. Wang, P. Qi, and H. Dai, "Measurement of ionizing radiation using carbon nanotube field effect transistor," *Phys. Med. Biol.*, vol. 50, pp. N23–N31, Jan. 1, 2005.

[13] C. D. Cress, C. M. Schauerman, B. J. Landi, S. R. Messenger, R. P. Raffaelle, and R. J. Walters, "Radiation effects in single-walled carbon nanotube papers," *J. Appl. Phys.*, vol. 107, no. 1, p. 014316, Jan. 1, 2010.

[14] W.-K. Hong, C. Lee, D. Nepal, K. E. Geckeler, K. Shin, and T. Lee, "Radiation hardness of the electrical properties of carbon nanotube network field effect transistors under high-energy proton irradiation," *Nanotechnol.*, vol. 17, no. 22, pp. 5675–5680, Jan. 1, 2006.

[15] S. A. Vitusevich, V. A. Sydoruk, M. V. Petrychuk, B. A. Danilchenko, N. Klein, A. Offenhausser, A. Ural, and G. Bosman, "Transport properties of single-walled carbon nanotube transistors after gamma radiation treatment," *J. Appl. Phys.*, vol. 107, no. 6, p. 063701, 2010.

[16] M. Hulman, V. Skakalova, S. Roth, and H. Kuzmany, "Raman spectroscopy of single-wall carbon nanotubes and graphite irradiated by gamma rays," *J. Appl. Phys.*, vol. 98, no. 2, p. 024311, Jan. 1, 2005.

[17] S. Yuan, Q. Zhang, D. Shimamoto, H. Muramatsu, T. Hayashi, Y. A. Kim, and M. Endo, "Hysteretic transfer characteristics of double-walled and single-walled carbon nanotube field-effect transistors," *Appl. Phys. Lett.*, vol. 91, no. 14, p. 143118, Jan. 1, 2007.

[18] M. Steiner, M. Freitag, J. C. Tsang, V. Perebeinos, A. A. Bol, A. V. Failla, and P. Avouris, "How does the substrate affect the Raman and excited state spectra of a carbon nanotube?," *Appl. Phys. A*, vol. 96, no. 2, pp. 271–282, Jan. 1, 2009.

[19] W. Kim, A. Javey, O. Vermesh, O. Wang, Y. Li, and H. Dai, "Hysteresis caused by water molecules in carbon nanotube field-effect transistors," *Nano. Lett.*, vol. 3, no. 2, pp. 193–198, Jan. 1, 2003.

[20] C. M. Aguirre, P. L. Levesque, M. Paillet, F. Lapointe, B. C. St-Antoine, P. Desjardins, and R. Martel, "The role of the oxygen/water redox couple in suppressing electron conduction in field-effect transistors," *Adv. Mater.*, vol. 21, no. 30, p. 3087, Jan. 1, 2009.

[21] C. Kocabas, M. Meitl, A. Gaur, M. Shim, and J. Rogers, "Aligned arrays of single-walled carbon nanotubes generated from random networks by orientationally selective laser ablation," *Nano. Lett.*, vol. 4, no. 12, pp. 2421–2426, Jan. 1, 2004.

[22] C. Kocabas, S. Dunham, Q. Cao, K. Cimino, X. Ho, H.-S. Kim, D. Dawson, J. Payne, M. Stuenkel, H. Zhang, T. Banks, M. Feng, S. V. Rotkin, and J. A. Rogers, "High-frequency performance of submicrometer transistors that use aligned arrays of single-walled carbon nanotubes," *Nano. Lett.*, vol. 9, no. 5, pp. 1937–1943, Jan. 1, 2009.

[23] M. S. Arnold, A. A. Green, J. F. Hulvat, S. I. Stupp, and M. C. Hersam, "Sorting carbon nanotubes by electronic structure using density differentiation," *Nature Nanotech.*, vol. 1, no. 1, pp. 60–65, Oct. 1, 2006.

[24] C. W. Lee, X. Dong, S. H. Goh, J. Wang, J. Wei, and L.-J. Li, "Illumination-enhanced hysteresis of transistors based on carbon nanotube networks," *J. Phys. Chem. C*, vol. 113, no. 12, pp. 4745–4747, Jan. 1, 2009.

[25] M. Engel, J. P. Small, M. Steiner, M. Freitag, A. A. Green, M. C. Hersam, and P. Avouris, "Thin film nanotube transistors based on self-assembled, aligned, semiconducting carbon nanotube arrays," *ACS Nano*, vol. 2, no. 12, pp. 2445–2452, Jan. 1, 2008.

[26] Z. Wu, Z. Chen, X. Du, J. Logan, J. Sippel, M. Nikolou, K. Kamaras, J. Reynolds, D. Tanner, A. Hebard, and A. Rinzler, "Transparent, conductive carbon nanotube films," *Science*, vol. 305, no. 5688, pp. 1273–1276, Jan. 1, 2004.

[27] M. C. LeMieux, M. Roberts, S. Barman, Y. W. Jin, J. M. Kim, and Z. Bao, "Self-sorted, aligned nanotube networks for thin-film transistors," *Science*, vol. 321, no. 5885, pp. 101–104, Jul. 4, 2008.

[28] W. J. Yu, U. J. Kim, B. R. Kang, I. H. Lee, E.-H. Lee, and Y. H. Lee, "Adaptive logic circuits with doping-free ambipolar carbon nanotube transistors," *Nano. Lett.*, vol. 9, no. 4, pp. 1401–1405, Jan. 1, 2009.

[29] P. Collins, K. Bradley, M. Ishigami, and A. Zettl, "Extreme oxygen sensitivity of electronic properties of carbon nanotubes," *Science*, Jan. 1, 2000.